BNL-63508

CONF-970201--5

FACTORS AFFECTING COERCIVITY IN RARE-EARTH-BASED ADVANCED PERMANENT MAGNET MATERIALS

L. H. Lewis
Materials Science Division, Department of Applied Science, Brookhaven National Laboratory, Upton, New York 11973-5000

C. H. Sellers
Idaho National Engineering Laboratory, Lockheed Martin Idaho Technologies Co., Idaho Falls, Idaho 83415-2211

V. Panchanathan
Magnequench International, Inc., 6435 Scatterfield Road, Anderson, Indiana 46013

Abstract

The relationships that link microstructural properties of advanced permanent magnet materials with magnetic properties such as the coercivity are often difficult to quantify, especially in materials with nano-scale structures. Recent work on $RE_2Fe_{14}B$-based powders fabricated with rapid-solidification techniques such as inert gas atomization (IGA) and melt-spinning provide insight into the nanostructural features which affect the acquisition and stability of coercivity. In all cases the coercivity is found to be a function of both the scale of the constituent microstructure and of the presence and distribution of minor phases.

Research was performed under the auspices of the U.S. Department of Energy, Division of Materials Sciences, Office of Basic Energy Sciences under Contract No. DE-AC02-76CH00016. Research was carried out in part at the National Synchrotron Light Source, Brookhaven National Laboratory, which is supported by the U.S. Department of Energy, Division of Materials Science and Division of Chemical Sciences. INEL work was supported through the Long-Term Research Initiative Program and DOE Division of Basic Energy Science under DOE Idaho Operations Office Contract DE-AC07-94ID13223.

Introduction

Coercivity, or "magnetic hardness", describes the ability of a magnetized magnetic material to resist the demagnetizing effects of an external field. Practically speaking, coercivity is an extrinsic property because in bulk materials it is determined largely by microstructural factors. The theoretical limit to coercivity is determined by a material's intrinsic anisotropy field H_k; however, in practice it is extremely difficult to attain coercivities even close to the anisotropy field because features such as microstructural defects and/or minor phases often provide low-energy routes for the nucleation of magnetic reversal.

Rare-earth-based permanent magnets, with coercivities H_{ci} generally exceeding 5000 Oe, are found in a very wide variety of applications, and the demand for rare-earth permanent magnets is growing by 10-15% per annum (1). Presently the largest demand for high-quality permanent magnets is found in the computer industry for disk-drive voice-coil motors; sensors and consumer electronics also utilize these magnets. The quality of permanent magnetic materials is quantified by the parameter "energy product", $(BH)_{max}$, which is determined by both extrinsic and intrinsic material parameters. The energy product is defined as the largest possible value of magnetic induction B multiplied by internal field H, (B·H), found in the second-quadrant (BH) demagnetization curve, and is thus determined by the remanence B_r and the coercivity H_{ci} of a given magnet. The energy product describes the amount of energy stored in a magnet and thus provides an estimation of its strength.

Today, the permanent magnet of choice for most of the above-described applications is based on the intermetallic compound $Nd_2Fe_{14}B$. Depending upon processing route and elemental additions, the $(BH)_{max}$ for commercial products can go as high as 45 MGOe; laboratory magnets with energy products as high as 50-52 MGOe have been reported (2). While these are strong magnets indeed, it is interesting to note that the theoretical energy product of $Nd_2Fe_{14}B$ is 64 MGOe, ~1.4 times the energy product of the best commercial magnets produced today. Realization of energy products closer to the theoretical values in magnets fabricated from the 2-14-1 composition would result in significant weight and size reductions in the components that use these magnets. One reason for the discrepancy between the theoretical and the actual energy product is due to deficiencies in coercivity: at room temperature, the remanence of aligned Nd-based 2-14-1 magnets is approximately 80% of the saturation magnetization, while the highest coercivities are only on the order of 30% of the anisotropy field (3).

The search for the links that connect coercivity with the microstructure is a challenging task that becomes increasingly so as the microstructural scale descends into the nanometer range, as is the case for magnetic materials fabricated by rapid solidification processing methods such as melt-spinning (4) and inert gas atomization (5). It has been empirically determined in a number of studies that coercivity in 2-14-1 materials produced by melt-spinning is a sensitive function of quench rate and hence, degree of crystallinity and crystallite size (4,6,7). Other factors that affect the coercivity are the presence, size and degree of crystallinity of minor phases as well as the orientational relationships amongst constituent major and minor phases. The extremely small scale of microstructures produced by rapid solidification techniques approaches that of domain walls widths in the materials and thus it is possible for exchange interactions, in addition to the ever-present magnetostatic interactions, to magnetically couple majority and minority phases. Such effects can create magnetic mesostructures that consist of many exchange-coupled grains, producing "interaction domains" (8,9) that are much larger than the individual crystallographically-defined grains. In many instances it is desirable to interrupt the exchange coupling between grains in order to isolate them magnetically and restore coercivity to that expected in single-domain material. However, in other instances the intergranular exchange coupling is exploited to create two-phase "exchange-spring" magnets (10) that consist of a magnetically soft phase intimately mixed with a hard phase to form a magnetic composite that possesses the best properties of each constituent phase. An unfortunate property of "exchange-spring" magnets fabricated thus far is that they al-

DISCLAIMER

ways possess a low coercivity, which renders them useful only for operations limited to the neighborhood of 80 °C (11). This deficiency exists in exchange-spring alloys fabricated in many laboratories, even though estimates of coercivity based on theoretical calculations indicate that it should be on the order of 25% of the theoretical coercive limit $2K_1/M_S$ (12).

New insights concerning factors that affect coercivity in magnetic materials fabricated by rapid solidification methods will be illustrated by recent results obtained from three types of magnetic materials, all based on the composition $Nd_2Fe_{14}B$ (2-14-1): magnetically-isotropic spherical powders produced by inert gas-atomization (IGA); thermomechanically-deformed and crystallographically-aligned (MQ-3) magnets, and powders of low rare-earth-content ("exchange-spring") alloys. It is hoped that new ideas of how to modify and control coercivity will result from detailed analyses of the microstructure-property interactions in these materials.

I. Particles Produced by Inert Gas Atomization

For many years, inert gas atomization (IGA) has been examined as a processing route for the production of rare earth permanent magnet materials such as $Nd_2Fe_{14}B$ (13-16). Similar to the commercially-viable technique of melt spinning, IGA involves rapid solidification from the melt and can result in a homogenous microstructure for fine powders. As in the case of melt-spun ribbons, gas-atomized powders are magnetically isotropic, potentially making them suitable for compaction into isotropic bonded and hot pressed magnets.

Previous efforts to produce IGA powders with suitable properties have been plagued by numerous problems which prevent their use in bonded magnets. One problem is the deleterious presence of α-Fe which lowers the coercivity in the final atomized product by providing low-anisotropy regions for reversal under relatively small reverse fields (17). Analysis of the phase diagram indicates that the 2-14-1 phase is a line compound and congruent solidification requires cooling rates that are typically higher than those normally achieved during gas atomization, which is on the order of $10^4 - 10^5$ K/sec. Atomization of alloy compositions similar to those used in melt spinning results in the precipitation of α-Fe because the cooling rate provided by IGA is too slow to bypass the properitectic α-Fe region. While the use of higher rare earth concentrations in the initial melt can produce powders with improved magnetic properties, such particles have an unsuitable coarse, multiphase microstructure in all but the finest powder size fractions (≈5 μm). A second drawback to the atomization of nominally-pure 2-14-1 alloys is that the product has an unacceptably high degree of crystallinity. In powders produced by melt-spinning, a homogeneous microstructure is achieved by quenching the melt at a rate sufficient to produce a structure which is overquenched, *i.e.*, at least partially amorphous, which is then heat-treated to yield a nanocrystalline structure with optimal magnetic properties. This level of cooling may be realized with the IGA process only for extremely fine (<5 μm) powders, prompting efforts to design atomization facilities which specifically produce powder batches that largely consist of such small powders. This route may result in a product which is susceptible to corrosion (because of the high surface-to-volume ratio), dangerous to handle (because of the pyrophoric nature of rare earth elements), and possesses unfamiliar bulk flow characteristics, requiring magnet manufacturers to redesign existing equipment for powder compaction into isotropic magnets.

An alternate approach for the improvement of the properties of IGA-processed $Nd_2Fe_{14}B$ powder is to alter the solidification characteristics of the melt itself to yield a product with a fine-scaled, homogeneous microstructure that persists to the larger-sized powder particles. It is found that the addition of specific elements — Ti and C — to the starting material increases the glass forming range of the 2-14-1 melt such that a large fraction of the as-quenched product possesses an amorphous or nanocrystalline structure. Since an increased proportion of the TiC-modified 2-14-1 powders exist in an overquenched state, relative to the unmodified powders, their magnetic properties may be more successfully optimized by brief annealing treatments.

Experimental Details:

Compositions near $RE_2Fe_{14}B$ were prepared from commercial grade materials by induction melting into an ingot. Several weight percent of Ti and C were also incorporated into some alloys at this point to alter the solidification characteristics (18). The ingot was broken up and induction melted at T ~ 1450 °C in the crucible of a small-scale gas atomizer using a close-coupled nozzle configuration with helium was as a cooling gas. The quenched powder size distribution was characterized by sonic sieving in air. In some cases powders were heat treated in an infrared vacuum furnace at 10^{-6} torr at 650 °C for a average of ten minutes. Magnetic properties of powders were determined with a vibrating sample magnetometer (VSM) after immobilization in wax and saturation in a capacitive magnetizer (6.5 Tesla field), as well as with a SQUID magnetometer using a maximum field of 5 T in the temperature range 10 K ≤ T ≤ 300 K; no demagnetization corrections were used. Powders were examined with a number of microscopy techniques: scanning electron microscopy (SEM) with standardless energy-dispersive spectroscopy (EDS); transmission electron microscopy (TEM) and tapping-mode magnetic force microscopy (MFM). Phase identification and analysis was done with x-ray diffraction using standard Cu-K_α radiation and at the National Synchrotron Light Source using x-ray wavelengths in the range 0.90 Å ≤ λ ≤ 1.19 Å, chosen so as to avoid the excitation of Fe fluorescence. Differential thermal analysis (DTA) was used to examine crystallographic and magnetic phase transformations as a function of temperature.

TiC-Modified *vs.* Unmodified $Nd_2Fe_{14}B$ IGA Particles

Over a period of several years many different alloy formulations have been atomized to determine the effect of composition, processing conditions, and atomizing gas on the powder microstructure and magnetic properties. The addition of Ti and C to the $Nd_2Fe_{14}B$ starting composition prior to atomization results in a fundamental change in the nature of the resultant melt, effectively reducing the quench rate necessary for the formation of the amorphous phase and thereby suppressing the formation of properitectic α–Fe. The microstructural and magnetic properties of the unmodified and the TiC-modified powders are discussed below:

Microstructure: In general, powders from both composition types have microstructures that depend on the cooling rate, which in turn depends upon the particle size. Large particles (> 100 μm) have an iron-rich dendritic microstructure which is surrounded by a rare-earth-rich matrix, with the volume fraction of the compositionally-distinct phases depending upon the specific particle size. Small particles (<1 μm) generally show an amorphous or nanocrystalline microstructure, attesting to their very rapid quench rate. The differences in the powder microstructure between the two composition types, however, are manifest in the intermediate particle size fractions, 5-75 μm. The atomized particle size distribution indicates a mean powder size of 50 microns in the unmodified 2-14-1 melt versus a mean powder size of 14 microns found in the TiC-modified material. Particles formed from the unmodified 2-14-1 composition show a distinctly crystalline character in the relatively small size fraction 10-20 μm, whereas the TiC-modified powders of this size range still possess a significant amorphous content. Fig. 1 shows SEM images of an as-quenched 20 μm-sized particle both with and without the TiC addition; the differences in crystallinity and macroscopic phase segregation are pronounced. DTA and XRD data show that the presence of a significant glassy component in the TiC-modified powders persists up to a size fraction of 75 - 100 μm. Pronounced differences in minor phase content between the two composition types are also apparent. Properitectic α-Fe is always detected by XRD in particles quenched from the unmodified composition, which is oxidized to form γ-Fe_2O_3 upon annealing (17). In contrast there is no XRD evidence of α-Fe in the TiC-modified particles; however, TEM investigation of submicron-sized particles shows the presence of α–Fe nanocrystallites in a glassy

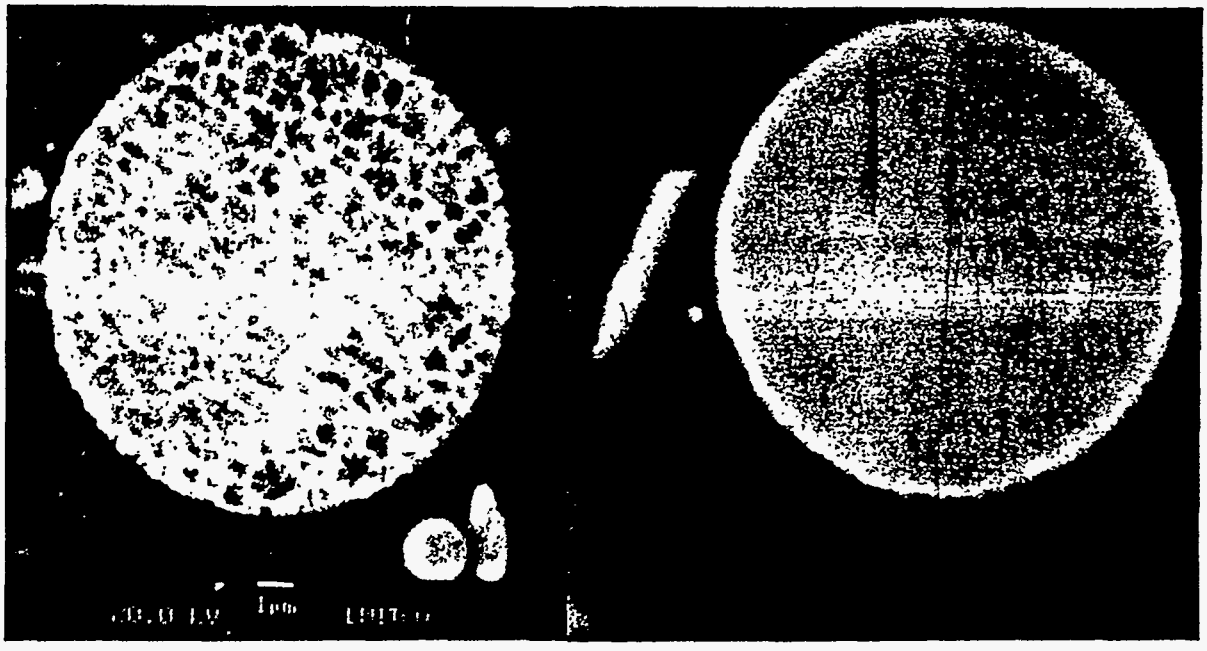

a). b).

Figure 1. SEM micrograph of as-atomized particles of equivalent size illustrating characteristic crystallinity difference: a). unmodified $Nd_2Fe_{14}B$ composition; b). TiC-modified composition.

matrix (19). As the TiC-modified as-quenched particle size is increased to 10-20 μm, the glassy matrix transforms to 2-14-1 grains with an average size of 60 nm, but the α-Fe phase is no long detected by TEM selected-area electron diffraction. TiC precipitates are found on the 2-14-1 intergranular boundaries in the TiC-modified IGA particles of larger size (>20 μm), in agreement with the results found in melt-spun ribbons of analogous composition (20). The powders appear to be nominally environmentally stable, suffering no loss in properties after exposure to normal laboratory conditions for 3 years. Auger electron spectroscopy indicates that a natural oxide layer is developed on the surface from trace impurity gases during atomization, such that no special handling or coating is necessary.

Magnetic Properties: A strong dependence of the magnetic properties on the powder size is noted for as-quenched powders produced from both composition types, a dependence that is reduced following heat treatment. The second quadrant of the room-temperature demagnetization curve from as-atomized TiC-free particles has a poor shape for all but the smallest (≈ 1 μm) sized particles, suggesting the presence of multiple magnetic phases. The alloys modified with TiC exhibit much softer magnetic properties in the as-quenched state, with coercivities H_{ci} near 100 Oe for the smallest particles. As the powder size increases for heat-treated TiC-free particles the energy product $(BH)_{max}$ always decreases with increasing particle size, Fig. 2(a). This is in contrast to the behavior of the TiC-modified particles for which a maximum in the energy product $(BH)_{max}$ is reached before decreasing again for the largest particles, Fig. 2(b). These results are consistent with the production of completely amorphous powders made from the TiC-modified composition in the finer size fractions, particles with an amorphous + microcrystalline structure up to the 75-100 μm size range, and particles with an underquenched (*i.e.*, crystalline) structure in the largest size range. This "bell" shaped dependence of the magnetic properties upon the cooling rate, via the powder size, is very reminiscent of the behavior observed in melt spun ribbons as the cooling rate is changed by alteration of the wheel speed.

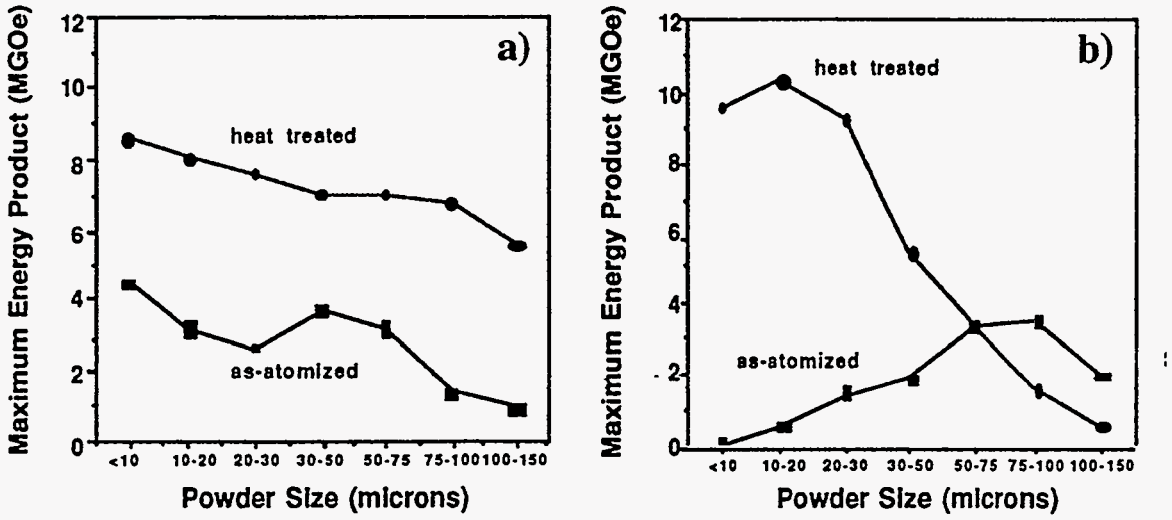

Figure 2. Powder particle size *vs.* energy product $(BH)_{max}$ for a). the unmodified (TiC-free) composition; b). the TiC-modified composition.

As in overquenched melt-spun ribbons, overquenched as-atomized IGA powders of both compositional types are easily crystallized by heat treatment to yield optimized magnetic properties. Although a much higher annealing temperature (T ≈ 800 °C) is needed to optimally crystallize the TiC-modified material, it is much less sensitive to the heat treatment temperature than materials prepared by melt-spinning or the unmodified IGA powders. In the TiC-free particles coercivities as high as 20 kOe may be found, depending upon the powder size, but the maximum energy products $(BH)_{max}$ do not exceed 7-9 MGOe after heat treatment. In contrast, upon heat treatment the the magnetic character of the TiC-modified powders in the < 30μm size transforms from magnetically-soft to to magnetically-hard and attain an energy product of 10.3 MGOe. From comparison with the much-studied behavior of melt-spun ribbon, this transformation indicates that the IGA particles of this size range are overquenched and/or amorphous. Upon annealing, the larger size fractions of IGA TiC-modified powder exhibit a decrease in $(BH)_{max}$, whereas the

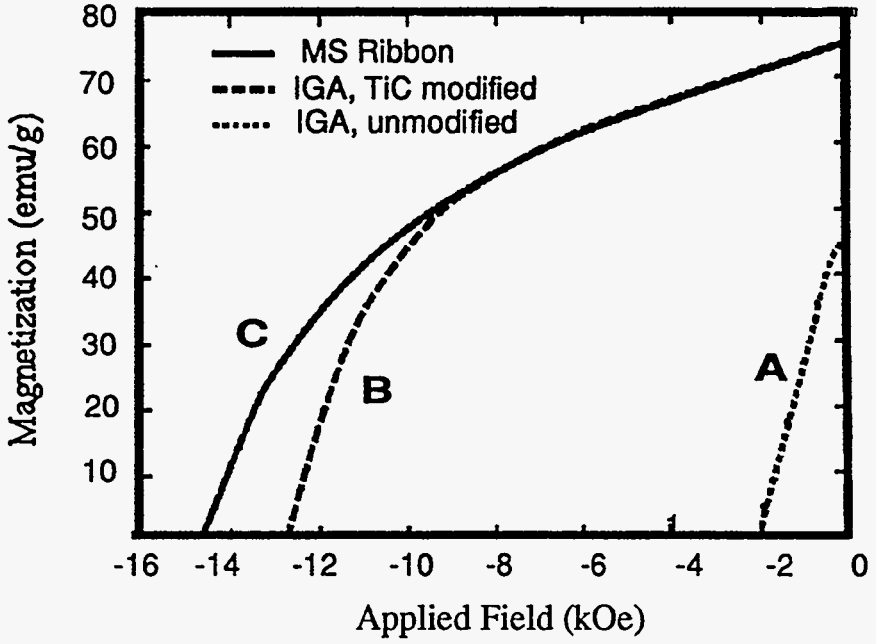

Figure 3. Second-quadrant demagnetization curves from annealed samples of a) TiC-free (unmodified) IGA powder; b) TiC-modified powder; c) commercial melt-spun ribbon.

larger size fractions of IGA unmodified powder exhibit an improvement in $(BH)_{max}$. This phenomenon is currently under investigation. While the gas-atomized TiC-modified alloy has a lower H_{ci} than the melt spun ribbon, B_r is unchanged, and $(BH)_{max}$ is quite high, Fig. 3. The ability to atomize alloy compositions with a lower rare-earth content (and consequently, a higher Fe content) with a fine microstructure results in an increase in B_r and $(BH)_{max}$ over that of the unmodified particles.

An important clue to the differences in the behavior of bonded magnets formed from powders produced from both compositions can be obtained from their domain structure as observed by MFM. The unmodified, TiC-free powder particle exhibits a coarse microstructure constituted of primary dendrite arms that contains many large (approximately 1 μm) domains. The MFM image of the TiC-modified powder particle shows a much smaller domain size and a uniform domain structure that has an unknown amount of correlation with the very fine microstructure. This domain structure resembles very closely that of optimally quenched melt spun ribbons (21) and appears to be responsible for the good performance of bonded magnets made from these new materials.

II. Effects of Minor Ferromagnetic Phases on Coercivity in Thermomechanically-Deformed $RE_2Fe_{14}B$-based Magnets

Although magnets based on the $RE_2Fe_{14}B$ compounds are more economical to manufacture than are other rare-earth-based magnetic compounds and exhibit impressive energy products, they also possess a high temperature coefficient of coercivity which causes the coercivity to fall steadily to unacceptably low values for temperatures much above 400 K. Any efforts to remedy this unfavorable coercivity behavior require the definitive identification of the dominant mechanism of magnetization reversal in these magnets, a topic that is still open to debate within the literature (22-26). In order to identify, understand and manipulate the reversal mechanism operative in the 2-14-1-based melt-quenched and thermomechanically-deformed (die-upset or MQ-3) magnets, it is necessary to investigate simultaneously the microstructural and the magnetic properties. Moreover, it is advantageous to study magnets formed from compounds that are largely free of the trace-level dopants such as Ga, Dy, Co, and Cu that are often added to commercial magnets, in order to reduce the experimental variables. To this end, a number of experiments have been performed on 2-14-1-based rare-earth magnets, both isotropic and aligned, obtained from the General Motors Research and Development Center with bulk compositions $Nd_{13.75}Fe_{80.25}B_6$ and $Pr_{13.75}Fe_{80.25}B_6$. Nanostructural and nanocompositional evidence obtained on these samples with high-resolution TEM methods coupled with investigations into the initial and high-temperature behavior of the magnetization reveals the presence of a previously-unobserved ferromagnetic grain boundary phase. The presence and distribution of this phase is expected to greatly affect the global reversal behavior and mechanism in these magnets. In related investigations, calculated hysteresis loops were fit to experimental loops obtained from the above-described materials using an algorithm based on the Jiles-Atherton theory (27). The calculated model parameters were correlated with the physical attributes of the magnets; interpretations of the information thus yielded provides substantial insight into the hypothesized reversal mechanisms and internal coupling found in these magnets. The results of all data obtained from studies of this set of melt-quenched, deformed magnets suggest that the dominant reversal mechanism is the nucleation of reversed domains.

Experimental Details:

Analytical electron microscopy was performed on the intergranular phases and the boundaries of deformed grains using both a VG Instruments HB-501 and a JEOL 2000 FX transmission electron microscope; the probe size used in the HB-501 instrument was on the order of 5 Å. Over

30 unique grain boundary regions were examined in the Pr-based sample while 10 were examined in the Nd-based sample (22, 28). Additional electron microscopy studies were done on the grain boundaries of these materials using a method based on high-resolution inner-potential-difference imaging and diffraction analyses (29). Magnetic investigations were performed with a SQUID magnetometer: initial magnetization curves and the dependence of the coercivity upon maximum magnetizing field at elevated temperatures in the temperature range 350 K $\leq$ T $\leq$ 425 K were examined (22). Each sample was sealed in an evacuated (P ~ 5 x 10^{-6} Torr) quartz capillary tube to avoid the possibility of oxidation during measurement (30). Prior to each minor loop measurement the magnets were thermally demagnetized by heating to 30 degrees above their nominal 2-14-1 Curie temperatures and then cooled in zero field to the measuring temperature; hysteresis loops were also measured at higher temperatures, 750 K - 800 K (31, 32).

Results and Discussion:

The microstructures of both the Nd-based and the Pr-based die-upset magnets are very similar. As described by other authors, (33, 34) the materials largely consist of highly anisotropic platelet-shaped grains of the 2-14-1 phase stacked parallel to their *c*-axes and separated from one another by a thin intergranular phase. The average dimensions of the deformed grains are 600 nm ± 150 nm in length by 150 nm ± 75 nm in width. The microstructures of the materials are surprisingly inhomogeneous and contain regions of large, undeformed grains. During the course of our studies it was found that the intergranular phase is amorphous and does not evenly wet all surfaces of the 2-14-1 grains; its presence is dependent upon the nature of the grain boundary in question. For example, there appears to be no intergranular phase in (001) twist boundaries parallel to the tetragonal basal plane. We found the average width of the intergranular phase to be 8 - 12 Å in the Nd-based magnet and 15 - 20 Å in the Pr-based magnet. Although previous researchers, using lower-resolution methods, have reported that the intergranular phase coats all surfaces and possess a composition close to the pseudobinary eutectic composition $RE_{70}Fe_{30}$, all high-resolution analytical electron microscope studies reported here clearly show that, for both the Nd-based and the Pr-based compositions, regions of the most narrow intergranular phase are enriched in iron relative to the bulk grain composition. Figure 4 a) illustrates the iron concentration profile in Pr-Fe-B upon traveling from one grain to another across the intergranular phase; it is to be noted that the iron concentration in the bulk grain is near 80%. Figure 4 b) gives a histogram of the relative ratio Fe:Pr in the grain boundary region versus that in the grain interior for a sampling of 30 grain boundaries. The trends for iron in the Nd-based sample were found to be very similar to those shown here for the Pr-based sample.

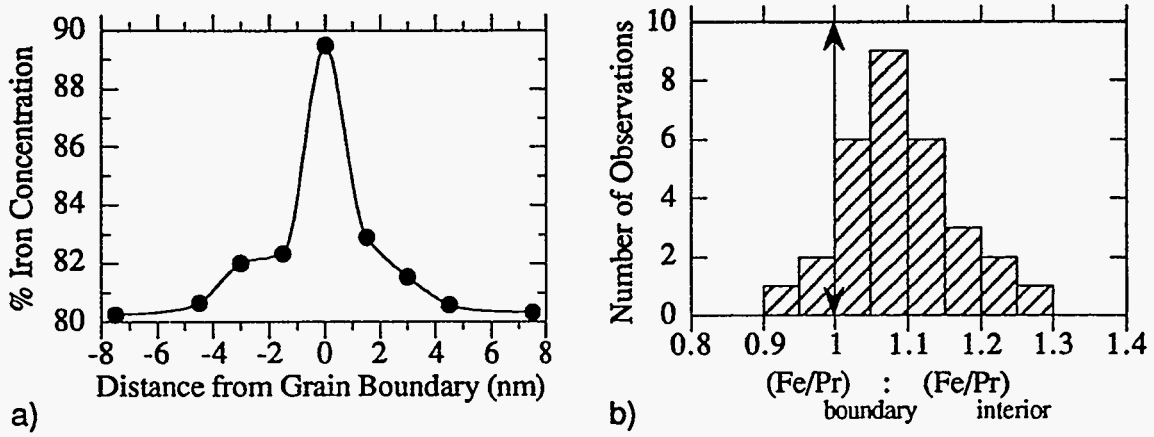

Figure 4. Quantitative results from analytical TEM performed on regions within the $Pr_{13.75}Fe_{80.25}B_6$ sample. a). Iron concentration as a function of distance from the grain boundary; b). Histogram depicting the Fe/Pr ratio for the grain boundary phase versus the grain interior. The arrow corresponds to the ratio value of 1 which signifies no depletion or enrichment in iron across the boundary.

The initial magnetization curves at various temperatures for Nd-Fe-B are illustrated in Fig. 5a); Fig. 5b) shows the development of the coercivity with maximum applied field; the results for the Pr-Fe-B sample look very similar. In all cases, the initial magnetization curves of both samples show a steep temperature-independent rise in the magnetization, followed by an approach to saturation that is temperature-dependent. The coercivities show the same trend, initially developing rapidly, with a common, temperature-independent slope that levels out to a constant, temperature-dependent value. These results are consistent with coercivity determined by nucleation: magnets with a high initial susceptibility have domain walls that move easily, implying that no domain-wall pinning occurs inside the crystallite (35). Additionally, in nucleation-dominated magnets the coercivity H_{ci} increases linearly with magnetizing field and then saturates, whereas in those magnets characterized by pinning the coercivity is almost negligible up to a critical field and then it suddenly increases to saturation (35). The common slope of the H_{ci} *vs.* H_a curve implies that these nucleation sites are structural features that are thermally sensitive. Fig. 6 shows a hysteresis loop from $Nd_{13.75}Fe_{80.25}B_6$ measured at T = 800 K. The sigmoidal shape of the high-temperature hysteresis loop indicates that another ferromagnetic phase, in addition to 2-14-1, is present in these materials; the size of this high-temperature magnetic signal is consistent with that expected from a ferromagnetic grain boundary phase with dimensions and distribution of that determined by the TEM studies (32).

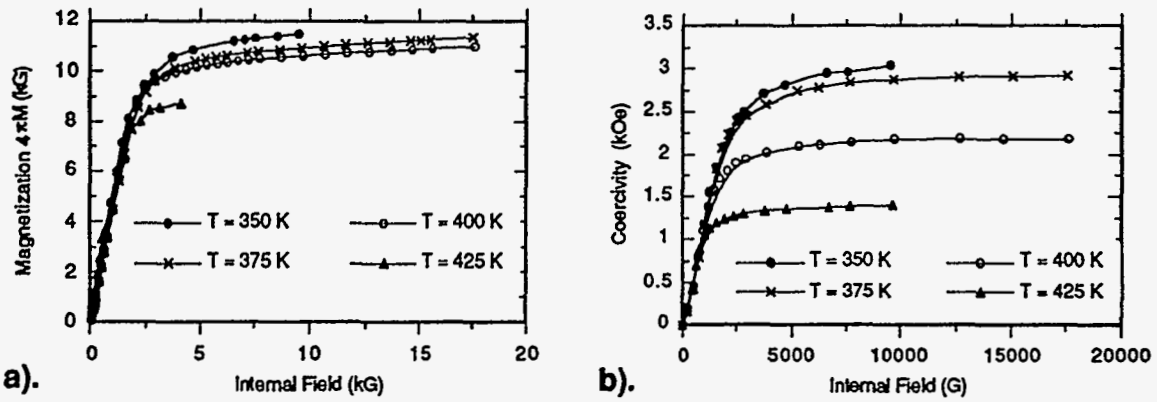

Figure 5. Magnetic data from the die-upset $Nd_{13.75}Fe_{80.25}B_6$ sample illustrating a). initial magnetization; b). development of coercivity H_{ci} with field.

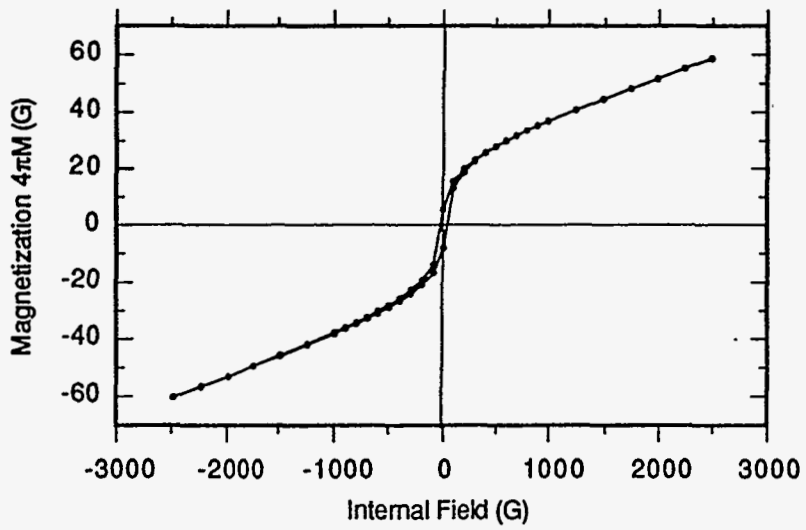

Figure 6. Hysteresis loop measured on die-upset $Nd_{13.75}Fe_{80.25}B_6$ at T= 800 K, above the Curie temperature of the 2-14-1 phase.

The micromagnetic origins of the coercivity in fine-grained material strongly depend upon the type of coupling between the grains. The presence of excess iron in the grain boundary phase has several important consequences with regards to intergrain interactions: the grains are likely to be exchange-coupled as well as magnetostatically coupled. Such a hypothesis would presuppose the existence of interaction domains, much like those observed by Kerr microscopy and MFM in similar melt-quenched, thermomechanically-deformed magnetic materials (37). Numeric micromagnetic calculations (38) of nucleation fields of 2-D magnetic structures demonstrate that if grains have direct exchange interactions, the entire sample can easily demagnetize after reversal of one grain.

Another possible consequence of the presence of a ferrous, ferromagnetic intergranular phase is the existence of lower-anisotropy sites for reverse magnetization nucleation. At the same time, such a characteristic may reduce the probability of domain wall pinning at the intergranular phase. However, it is recognized that pinning must be operative also: as stated by Livingston (39), pinning is a necessary requirement, even in nucleation-controlled magnets, to avoid catastrophic reversal originating at low-coercivity regions. A likely place for pinning to occur is at the larger RE-rich non-magnetic particle pockets found along some of the grain boundaries and at grain-boundary triple points (22, 28, 34). Although our results concerning the microstructure of these magnets differ considerably from those of previous researchers (33, 34) obtained by lower-resolution methods, we do not doubt that a phase with a composition close to $Nd_{70}Fe_{30}$ does exist in these materials, especially since the excess rare-earth present in these magnets must be present somewhere in the microstructure. However, the exact distribution within the microstructure of rare-earth-rich and iron-rich grain boundaries, as well as intragranular phases, remains to be determined.

The above experimental results suggest methods to improve the temperature coefficient of coercivity in die-upset $RE_2Fe_{14}B$ magnets. An ideal microstructure for a nucleation-type magnet consists of grains of a magnetically hard phase that are exchange-isolated from one another (39). Therefore, segregation of non-magnetic atoms to the grain-boundary phase via metallurgical manipulation would be expected to produce higher-coercivity magnets via destruction of the ferromagnetic exchange coupling. This argument is supported by the results obtained from hysteresis loops calculated from an algorithm based on the Jiles-Atherton theory (27). The Jiles-Atherton theory is based on considerations of the dependence of energy dissipation within a magnetic material resulting from changes in its magnetization. Model parameters were calculated from the algorithm and linked with the physical attributes of a set of three related melt-quenched permanent magnets based on the $Nd_2Fe_{14}B$ composition: hot-pressed (MQ-2) $Nd_{13.75}Fe_{80.25}B_6$, die-upset (MQ-3a) $Nd_{13.75}Fe_{80.25}B_6$ and elementally-modified die-upset (MQ-3b) $[Nd_{13}(Fe_{0.95}Co_{0.05})_{81}B_6]_{0.996}Ga_{0.004}$ (9). The measured room-temperature saturation magnetizations, remanences and intrinsic coercivities were used as inputs into the model to reproduce the experimental hysteresis curves. The calculated results show that two of the calculated parameters, the saturation magnetization M_S and the effective coercivity k, agree well with their directly-determined analogs. The calculated a and α parameters, which are interpreted to represent the "effective domain" density and the mean exchange coupling strength between the "effective domains", provide support for the concept of increased intergranular exchange-coupling upon thermomechanical deformation, and decreased intergranular exchange-coupling with the addition of gallium. The notion of the "effective domains" may be associated or equated with that of interaction domains. For example, the decrease in the a parameter from the relatively high value of 13920 Oe in MQ-2 sample to the low value of 1247 Oe in MQ-3(a) sample represents a decrease in the density of effective domains, which is consistent with a change in the microstructure that promotes exchange coupling among the grains in the die-upset sample, as would be expected if a significant portion of intergranular phase changed in composition from rare-earth-rich to iron-rich. The increase of the a parameter in DU2162, the sample doped with both cobalt and gallium, relative to that of DU1418, is consistent with a certain amount of exchange decoupling between

the grains that serves to produce a greater density of "effective domains". Many researchers (40-43) believe that when gallium is added to 2-14-1-based magnets it segregates to the grain boundary phase; such a segregation would be expected to decrease the intergranular coupling by diluting the magnetic properties of the intergranular phase.

III. Investigations Into Coercivity Mechanisms in "Exchange-Spring" Nd-Fe-B Alloys

Some researchers (44) believe that the next generation of permanent magnets may not stem from an as-yet undiscovered intermetallic composition but rather will be a magnetic composite comprised of an aligned hard-magnet skeleton phase filled in with a soft-magnetic phase of high saturation magnetization, known as an aligned "exchange-spring" magnet (10). Micromagnetic calculations (45) indicate that energy products in suitably-structured $Sm_2Fe_{17}N_3/Fe_{65}Co_{35}$ aligned magnets may reach 137 MGOe. Even isotropic two-phase "exchange-spring" permanent magnets hold great commercial promise if they can be fabricated so as to take full advantage of the optimal properties of each constituent phase. However, in practice it seems that such composites always possess a low coercivity, regardless of method of fabrication or elemental make-up. Both experimental (46, 47) and theoretical (48-50) studies conclude that the coercivity is a sensitive function of the dimension of the soft phase. Theoretical calculations indicate that ideal exchange-spring magnets should possess coercivities on the order of 25% of the theoretical coercive limit $2K_1/M_S$ (12), where K_1 is the first-order anisotropy constant and M_S is the saturation magnetization. The disparity between theoretical and empirical results indicates that the details of the interactions inherent to real magnets are not represented perfectly in the modeling efforts.

Experimental Details:

To clarify factors affecting coercivity, investigations were performed on the nature and evolution of the magnetic interactions in three 2-14-1/α-Fe magnetic composites that differ in the α-Fe phase content. The alloys were made from commercial-grade materials by standard melt-quenching techniques and were annealed for four minutes at 690 °C to optimize their magnetic properties. The starting compositions are given in Table I in both wt% and stoichiometry; henceforth the alloys will be identified by their excess iron enrichment δ, defined as $Nd_2Fe_{14+\delta}B$. Powders were verified by synchrotron x-ray diffraction (XRD) using $\lambda \approx 0.90$ Å - 1.18 Å to consist of only two phases: $Nd_2Fe_{14}B$ and α-Fe. Lattice parameters (Table I) were obtained using a least-squares-fit algorithm, and the approximate particle size was determined with the Scherrer formula from the peak full-width at half-maximum. Magnetic measurements were made on isotropic cylindrical powder compacts in the temperature range $275K \leq T \leq 350K$ with a MPMS SQUID magnetometer. The data were corrected for demagnetization effects, and room-temperature demagnetization curves were extrapolated to an infinite internal field to calculate the remanence enhancement. Isothermal remanent magnetization (IRM) studies (51) monitored the development of the coercivity and magnetization from an *ac*-demagnetized state. DC-demagnetization (DCD) studies (51) were done on samples saturated at -5 T and then subjected to increasingly positive fields until reversal and saturation in the positive direction was achieved. The reversible ($M_{rev}(H)$) and irreversible ($B_r(H)$) components of the magnetization were determined with the relation $M_{tot}(H) - B_r(H) = M_{rev}(H)$, where $B_r(H)$ is the value of the remanence at zero internal field and $M_{tot}(H)$ is the measured magnetization. The data are often represented by the susceptibility χ, where $\chi = \frac{\partial M}{\partial H_{int}}$, which provides an easily-visible signal with which to monitor the magnetization changes.

Table I: Alloy Characterization. δ characterizes the iron enrichment, defined as $Nd_2Fe_{14+\delta}B$.

Sample/ Stoichiometry	Composition (RE = rare earth)	2-14-1 Lattice Parameters (Å)	Grain Sizes	Remanence Ratio(B_r/M_S)
MQP-A (δ=0) $Nd_{2.39}Fe_{14}B_{0.95}$	RE = 30 wt% B = 0.9 wt% Fe = 68.6 wt%	a = 8.8042±.0020 c = 12.2608±.0046	2-14-1: ≈ 300 Å	0.53
MQ182 (δ=4.6) $Nd_2Fe_{18.6}B_{2.38}$	RE = 21.3 wt% B = 1.90 wt% Fe = 76.8 wt%	a = 8.7905±.0012 c = 12.1697±.0023	2-14-1: ≈ 500 Å α-Fe: ≈ 130 Å	0.52
MQ174 (δ=9.3) $Nd_2Fe_{23.3}B_{1.45}$	RE = 18 wt% B = 0.99 wt% Fe = 81.0 wt%	a = 8.8052±.0023 c = 12.2135±.0053	2-14-1: ≈ 300 Å α-Fe: ≈ 150-250Å	0.60

Results and Discussion:

Table I shows that the three samples studied possess similar, but not identical, lattice constants and average constituent phase sizes. The alloys have smooth second-quadrant demagnetization curves and exhibit a modest remanence enhancement compared to the value of 0.5 calculated for an isotropic compact of isolated particles. It was not possible to *ac*-demagnetize the δ = 0 sample in this study, therefore no IRM data from this sample are displayed.

The reversible and irreversible parts of the magnetization and their derivatives reveal the nature of magnetic reversal. The irreversible part of the magnetization describes the relative ratio of reversed grains or domains as a function of internal field and is, by definition, associated directly with the coercivity. By extension, the irreversible susceptibility χ_{irr} depicts the degree of collectiveness of the reversal process: very narrow χ_{irr} peaks indicate a highly collective reversal that occurs at one well-defined field, whereas broad and χ_{irr} peaks signal a non-collective reversal process that extends over a large field range. Figs. 7 a)-c) display the irreversible components of the susceptibility, χ_{irr} (DCD) and χ_{irr} (IRM), at various temperatures. The trends observed in the development of χ_{irr}(IRM) (Fig. 7 b), c)) are also evident in the development of coercivity with field, Fig. 8. Both figures indicate that the domain reversal from a demagnetized (IRM) state in the two-phase alloys is bimodal and broad, signifying that two processes are present and operate over an extended field range. The two χ_{irr} (IRM) maxima likely stem from the two constituent phases of the alloy: the low-field maximum in the vicinity of $H_{int} \approx 2000$ G corresponds to the reversal of the soft α-Fe phase, whereas the higher-field maximum around $H_{int} \approx 4000$ G corresponds to the reversal of the hard 2-14-1 phase. Equivalent conclusions have been drawn by Feutrill *et al.* (52) on similar materials. The reversible magnetization component M_{irr} for both DCD and IRM processes is shown in Fig. 9 for various temperatures as a function of internal field. The maximum amount of DCD reversible magnetization increases with the α-Fe content in the alloy, and temperature increases cause the peaks to sharpen up and move to lower fields. (The M_{irr} (IRM) data are shown only for T = 300 K because they exhibited very little temperature dependence; M_{rev} (DCD) for the δ = 0 sample is small up to 5 T.)

Once all the grains are magnetically aligned (*i.e.*, in a saturated state), Fig. 7a), the peaks of M_{irr} (DCD) and the coercivity H_{ci} are no longer bimodal and occur at precisely the same fields as do the peaks in the M_{rev} (DCD) signals. These results demonstrate that the two constituent phases in the sample reverse coherently, *i.e.*, are exchange-coupled. The heights of the DCD χ_{irr} data exceed those of the analogous IRM data by approximately 50 times, Fig. 7, much larger than the factor of two that describes interactionless process (53). In contrast, the χ_{irr} (DCD) data of the

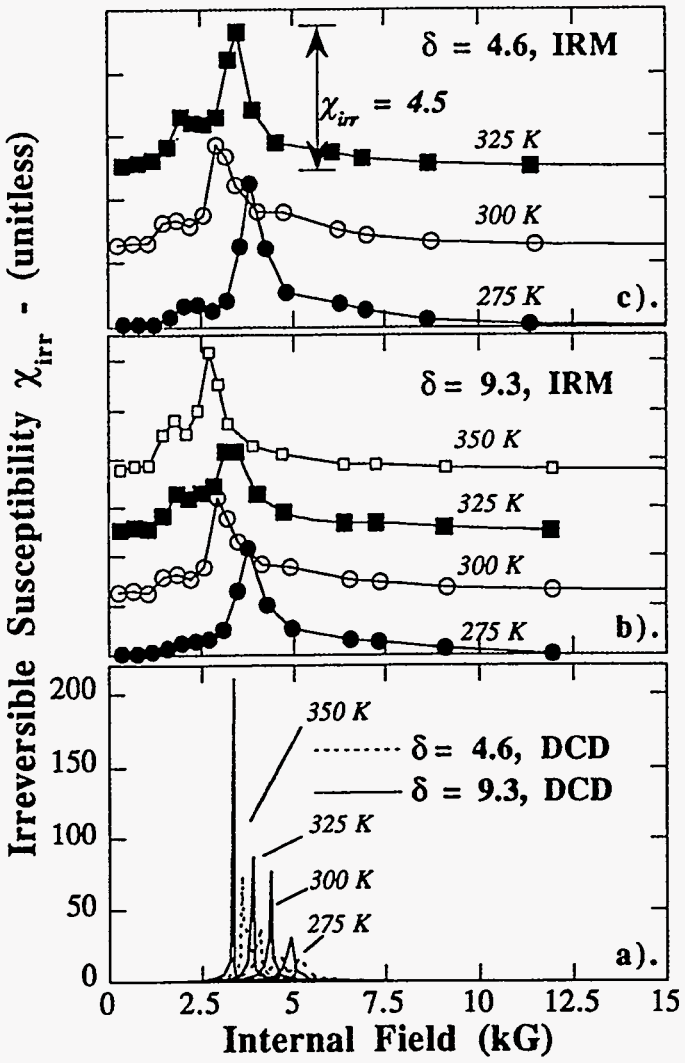

Figure 7. a). DCD (dc-demagnetization) curves for the δ = 4.6 and δ = 9.3 samples at various temperatures. b). IRM (isothermal remanent magnetization) curves for the δ = 9.3 sample at various temperatures. c) IRM curves for the δ = 4.6 sample at various temperatures. The measured height of a representative curve is included for reference.

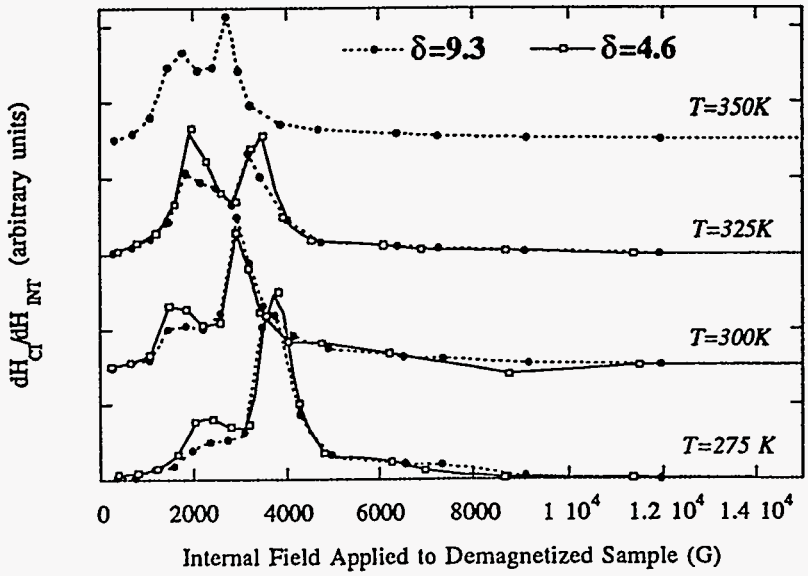

Figure 8. Development of coercivity with internal field applied to the ac-demagnetized samples δ = 9.3 and δ = 4.6.

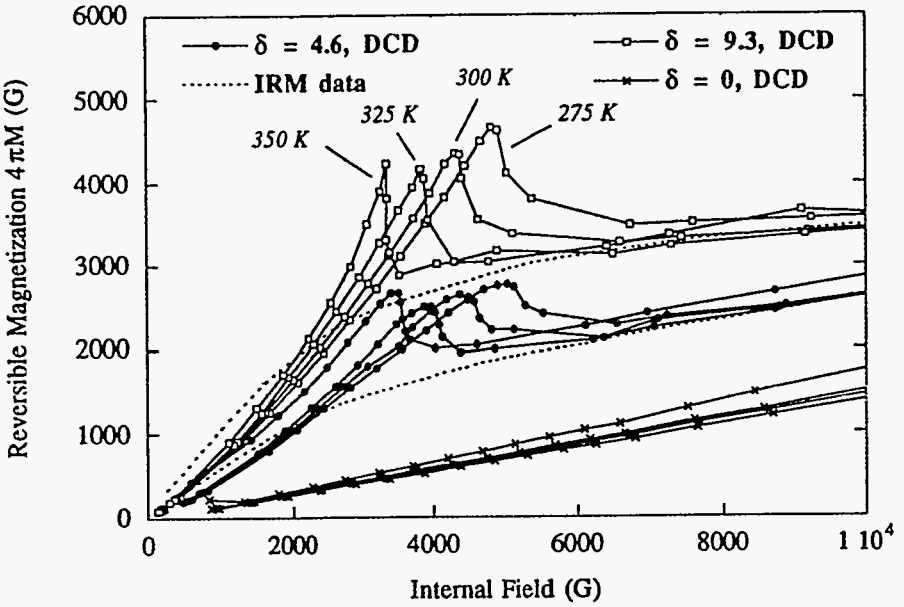

Figure 9. The reversible magnetization M_{rev}(DCD) and M_{rev}(IRM) as functions of internal field and temperature.

nominally single-phase sample $\delta = 0$ show very broad peaks ($\approx$ 10 kG) with a maximum susceptibility value of 5 that occurs in the range 10 kG $\leq H \leq$ 15 kG.

Fig.10 shows the dependence of χ_{irr} on temperature and internal field, along with the theoretical anisotropy fields ($\approx 2K_1/M_S$) for α-Fe (54) and $Nd_2Fe_{14}B$ (55); all data have been normalized to their values at 275 K. The approximate room-temperature values of the anisotropy fields of α-Fe and $Nd_2Fe_{14}B$ are 150 Oe and 89500 Oe, respectively.

The exchange coupling in these alloys is due to the α-Fe phase, manifest in the behavior of the irreversible magnetization M_{irr}, Fig. 8. Current theoretical models (48-50) all emphasize that the nanocomposite phases will be exchange-coupled if the dimension of the soft phase does not exceed the domain wall width in the hard phase. Reversal from a saturated state is hypothesized

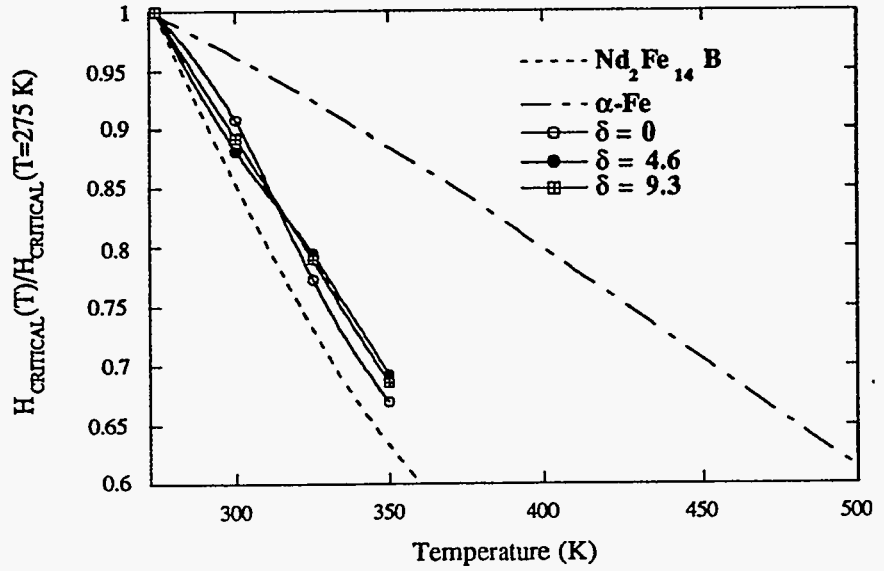

Figure 10. Normalized critical fields for reversal from a saturated state as a function of temperature.

to initiate in the exchange-isolated center of the soft phase and catastrophically proceed throughout the sample when the internal field exceeds the nucleation field of the magnetically-soft phase, H_N, which is computed to decrease as the size of the soft precipitates increases. However, the results of this study indicate that the critical reversal field H_N cannot be a simple function of the constituent phase anisotropy fields. Fig. 9 illustrates that both the temperature dependence of the anisotropy and the values of the critical reversal field of the alloys are intermediate to those of the pure constituent phases, but closer to that of $Nd_2Fe_{14}B$. If reversal does initiate in the exchange-isolated regions of the soft α-Fe precipitates, it would be expected that the temperature dependence of χ_{irr} (DCD) would more resemble that of pure α-Fe; however, the temperature dependence is closer to that of the 2-14-1 phase. Thus it appears that the hard 2-14-1 phase participates in the irreversible magnetic reversal even at very low fields, a conclusion also reached by other researchers (56).

To explain this phenomenon it is hypothesized that a nanostructural feature, such as a gradual crystallographic or chemical transition between the two phases, produces a region with a gradually-changing anisotropy constant of intermediate value. While preliminary electron microscopy performed on other samples with similar compositions (57) has not found such a proposed phase, it is likely to be manifest in other effects: for example, Dahlgren *et al.* (58, 59) investigated the spin reorientation temperature T_S of compositionally-related nanocomposite samples with ac susceptometry and found that T_S was depressed relative to the value found in single-crystal $Nd_2Fe_{14}B$ by as much as 17 degrees.

Summary

Recent results obtained from the three types of rapidly-solidified materials based on the $RE_2Fe_{14}B$ compound illustrate how the scale of the microstructure as well as the presence and nature of secondary phases can affect coercivity. Such knowledge may then be used to manipulate the detailed microstructure of the material to yield desired coercivities. The rapid-solidification process of inert gas atomization (IGA) has proven to be a promising method to produce $RE_2Fe_{14}B$-based isotropic magnetic powders with acceptable coercivity values. To compensate for the relatively slow quench rate provided by this method it has proven necessary to alter the composition of the starting material in order to increase the quenchability of the melt. It has been demonstrated that elemental additions of Ti and C alter the solidification process of the melt such that a large fraction of the atomized product is produced in the overquenched state, ready to be optimized into nominally single-domain-sized nano-scale grains by judicial heat treatment. The discovery of a ferromagnetic grain boundary phase in thermomechanically-deformed melt-quenched (MQ-3) magnets of selected compositions not only requires the alteration of some prevalent concepts of the micromagnetic organization of such systems, but also reveals possible metallurgical schemes with which to alter the coercivity of the system. Measurements of the temperature dependence of irreversible magnetization in two-phase "exchange-coupled" magnets indicate that the detailed of the exchange coupling between the constituent phases — $Nd_2Fe_{14}B$ and α-Fe — is more complicated than previously thought. In specific, it appears that all stages of reversal are largely governed by the 2-14-1 hard phase, with the α-Fe phase playing a relatively minor role. It is clear that new ideas must be explored to define the interactions that govern the magnetic behavior in this new class of magnetic materials.

References:

1. W. G. Hart, A. C. Nyce, H. D. Olmstead, and P. Wheeler, "Current Status and Future Growth of the Global Magnetic Materials Industry," Gordon International Consulting Conference on NdFeB 95: New Technologies, New Applications, New Markets (San Diego, California, 26-28 February 1995).

2. J. J. Croat, "Current Status of Rapidly Solidified NdFeB Permanent Magnets," 13th International Workshop on Rare Earth Magnets and Their Applications, (Birmingham, England, 1994) 65-78.

3. J. F. Herbst, "$R_2Fe_{14}B$ Materials: Intrinsic Properties and Technological Aspects," Rev. Mod. Phys. 63 (4) (1991) 819-898.

4. J. J. Croat, J. F. Herbst, R. W. Lee and F. E. Pinkerton, "Pr-Fe and Nd-Fe-based Materials: A New Class of High-Performance Magnets," J. Appl. Phys. 55 (1984) 2078-2082.

5. D. J. Branagan, T. A. Hyde, C. H. Sellers and R. W. McCallum, "Developing Rare Earth Permanent Magnet Alloys for Gas Atomization," J. Phys. D.: Appl. Phys. 29 (1996) 2376-2385.

6. H. Kronmüller, K.-D. Kurst and M. Sagawa, "Analysis of the Magnetic Hardening Mechanism in RE-FeB Permanent Magnets," J. Magn. Magn. Mater. 74 (1988) 291-302.

7. Akira Higuchi and Satoshi Hirosawa, "Sintered Nd-Fe-B Permanent Magnets," IEEE Trans. Magn. 25 (1989) 3555-3560

8. F. Pinkerton, "Evidence for Particle Interaction Effects in Nd-Fe-B Ribbons," J.Appl. Phys. 63 (11) (1988) 5427-5432.

9. L. H. Lewis, J. Gao, D. C. Jiles and D. O. Welch, "Modeling of Permanent Magnets: Interpretation of Parameters Obtained from the Jiles-Atherton Hysteresis Model", J. Appl. Phys. 79 (8) (1996) 6470-72.

10. Eckart F. Kneller and Reinhard Hawig, "The Exchange-Spring Magnet: A New Material Principle for Permanent Magnets," IEEE Trans. Magn. 27 (4) (1991) 3588-3600

11. V. Panchanathan, "Studies On Low Rare-Earth Nd-Fe-B Compositions," IEEE Trans. Magn. 31 (6) 3605-3607 (1995)

12. T. Schrefl, H. Kronmüller, J. Fidler, "Exchange Hardening in Nano-Structured Two-Phase Permanent Magnets," J. Magn. Magn. Mater. 127 (1993) L273-L277.

13. M. Yamamoto, A. Inoue, and T. Masumoto, "Productionof Nd-Fe-B Alloy Powders Using High-Pressure Gas Atomization and Their Hard Magnetic Properties," Met. Trans. A 20A, 5-11 (1989).

14. C.J. Williams, E.J. Dulis, and F.S. Snyder, U.S. Patent 4,994,109, "Method for Producing Permanent Magnet Alloy Particles for Use in Producing Bonded Permanent Magnets", Feb. 19, 1991.

15. I.E. Anderson, B.K. Lograsso, and R.W. McCallum, Proceedings of the First International Conference on Processing of Materials for Properties, eds. H. Henein and T. Oki, 645 (TMS Publications, 1993).

16. Z.S. Wronski, "MIcrostructure and Magnetic Properties of Low-Neodymium Nd-Fe-B-Si Magnets Produced from HP Gas Atomized Powder," J. Appl. Phys. 69, 5507-5509 (1991).

17. L. H. Lewis, C. H. Sellers, V. Panchanathan, "Annealing-Induced Property Improvements in 2-14-1 Powders Produced by Inert Gas-Atomization", IEEE Trans. Magn, in press.

18. D.J. Branagan and R.W. McCallum, "Altering the Cooling Rate Dependence of Phase Formation During Rapid Solidification in the $Nd_2Fe_{14}B$ System," J. Magn. Magn. Mater. 146, (1995) 89-102.

19. J.-Y. Wang, L. H. Lewis, Y. Zhu, D. O. Welch, C. H. Sellers, D. J. Branagan, V. Panchanathan, "Transmission Electron Microscopy of Inert Gas-Atomized Particles Based on the $Nd_2Fe_{14}B$ Composition: Effect of Alloying Additions", accepted in J. Appl. Phys.

20. D. J. Branagan, C. H. Sellers, M.J. Kramer, K. W. Dennis and R. W. McCallum, "A Metallurgical Approach Toward Alloying Applied to Rapid Solidification Processing of Rare Earth Permanent Magnet Systems," to be presented at the ASM-TMS Materials Week '96, Cincinnati, Ohio, 7-10 October 1996.

21. D.J. Branagan, T.A. Hyde, C.H. Sellers, and L.H. Lewis, "A New Generation of Gas Atomized Powder with Improved Levels of Energy Product and Processability," IEEE Trans. Magn., in press.

22. L. Henderson Lewis, Y. Zhu and D. O. Welch, "Evidence for Reversal by Nucleation in RE-Fe-B Die-Upset Magnets," J. Appl. Phys. 78 (10) (1994) 6235-6237.

23. L. Folks, R. Street and R. Woodward, "Investigation of Interaction Mechanisms in Melt Quenched NdFeB," J. Appl. Phys. 75 (1993) 5751-5753.

24. F. E. Pinkerton and C. D. Fuerst, "A Strong Pinning Model for the Coercivity of Die-Upset Pr-Fe-B Magnets," J. Appl. Phys. 69 (1991) 5817-5819.

25. D. Givord, Q. Lu, M. F. Rossignol, P. Tenaud and T. Viadieu, "Experimental Approach to Coercivity Analysis in Hard Magnetic Materials," J. Magn. Magn. Mater.83 (1990) 183-188.

26. M. Grönefeld and H. Kronmüller, "Initial Magnetization Curve and Hardening Mechanism in Rapidly Quenched Nd-Fe-B Magnets," J. Magn. Magn. Mater. 88 (1990) L267-L274.

27. D. C. Jiles and D. L. Atherton, "Theory of Ferromagnetic Hysteresis," J. Magn. Magn. Mater. 61 (1986) 48-60.

28. Tai D. Nguyen, Kannan M. Krishnan, Laura Henderson Lewis, Yimei Zhu and David O. Welch, "Microstructure and Composition in Rapidly Quenched NdFeB-based Hard Magnet Alloys," J. Appl. Phys. 79 (8) (1996) 4848-4850.

29. Yimei Zhu, J. Tafto, L. H. Lewis and D. O. Welch, "Electron Microscopy of Grain Boundaries: An Application to RE-Fe-B (RE=Pr or Nd) Magnetic Materials," Phil. Mag. Lett. 71 (1995) 297-305

30. L. H. Lewis and Konrad M. Bussmann, "A Sample Holder Design and Calibration Technique for the Quantum Design MPMS SQUID Magnetometer," Rev. Sci. Instrum., in press.

31. L. Henderson Lewis, Yimei Zhu and D. O. Welch, "Ferromagnetic Grain Boundary Signature in Die-Upset RE-Fe-B Magnets," Scripta Met. Mat. 33 (10/11) (1995) 1775-1780

32. L. H. Lewis, D. O. Welch and F. Pourarian, "Quantitative characterization of additional ferromagnetic phase in melt-quenched and sintered Nd-Fe-B-based magnets", J. Appl. Phys. 79 (8) 5513-15 (1996)

33. T.-Y. Chu, L. Rabenberg and R. K. Mishra, "Evolution of the Microstrucutre of Rapidly Solidified Nd-Fe-B Permanent Magnets" J. Appl. Phys. 69 (8) (1991) 6046-6048.

34. R. K. Mishra, "Microstrucutre of Hot-Pressed and Die-Upset NdFeB Magnets," J.Appl. Phys. 62 (1991) 967-971.

35. G. Hadjipanayis and A. Kim, "Domain Wall Pinning versus Nucleation of Reversed Domains in R-Fe-B Magnets," J. Appl. Phys. 63 (1988) 3310-3315

36. L. Folks, R. Street and R. C. Woodward, "Observation of Domains in a Die-Upset Melt-Spun Magnet," 13th International Workshop on Rare Earth Magnets and Their Applications, (Birmingham, England, 1994).

37. T. Schrefl, H.F. Schmidts, J. Fidler, H. Kronmüller, "Nucleation of Reversed Domains at Grain-Boundaries," J. Appl. Phys. 73 (10) 6510-6512 (1993)

38. J. D. Livingston, "Nucleation Fields of Permanent Magnets," IEEE Trans. Magn. MAG-23 (1987) 2109-2113.

39. R. Ramesh and G. Thomas, Mater. Sci. Eng. B 3, (1989) 435.

40. V. Panchanathan and J. J. Croat, "Properties of Rapidly Solidified Nd-Fe-Ga-B Alloys," IEEE Trans. Magn. 25 (1989) 4111

41. M. Tokunaga, Y. Nozawa, K. Iwasaki, M. Endoh, S.Tanigawa and H. Harada, "Ga Added Nd-Fe-B Sintered and Die-Upset Magnets," IEEE Trans. Magn. 25 (1989) 3561

42. C. D. Fuerst and E. G. Brewer, "High-Remanence Rapidly Solidified Nd-Fe-B - Die-Upset Magnets," J. Appl. Phys. 73 5751-5756 (1993)

43 I. Ahmad, H. A. Davies, R. A. Buckley, "Ultra-High Coercivity Nd-Fe-B Permanent-Magnet Alloy With Small Addition Of Ga,"Mater. Lett. 20 (3-4) 139-142 (1994)

44. R. Skomski and J. M. D. Coey, "Giant Energy Product in Nanostructured 2-Phase Magnets," Phys. Rev. B 48 (1993) 15812-15816

45. R. Skomski, "Aligned Two-Phase Magnets: Permanent Magnetism of the Future?," J. Appl. Phys. 76 (10) (1994) 7059-7064.

46. G. C. Hadjipanayis, L. Withanawasam and R. F. Krause,"Nanocomposite $R_2Fe_{14}B/\alpha$-Fe Permanent Magnets," IEEE Trans. Magn. 31 (6) (1995) 3596-3601

47. J. M. Yao, T. S. Chin and S. K. Chen, "Coercivity of Ti-Modified (α-Fe) - $Nd_2Fe_{14}B$ Nanocrystalline Alloys," J. Appl. Phys. 76 (10) (1994) 7071 -7073

48. R. Fischer, T. Schrefl, H. Kronmuller and J. Fidler, "Phase Distribution and Computed Magnetic Properteis of High-Remanent Composite Magnets," J. Magn. Magn. Mater. 150 (1995) 329-344

49. E. H. Feutrill, P. G. McCormick and R. Street, "Simulation of Magnetization Reversal in 2-Phase Exchange-Coupled Nanocrystalline Materials, " J. Appl. Phys. 75 (10) (1994) 5701-5703.

50. H. Fukunaga and H. Inoue, "Effect of Intergrain Exchange Interaction on Magnetic Properties in Isotropic Nd-Fe-B Magnets," Jpn. J. Appl. Phys. 31 Pt. 1 (5A) (1992) 1347-1352.

51. P.E. Kelly, K. O'Grady, P. I. Mayo and R W. Chantrell, "Switching Mechanisms in Cobalt-Phosphorus Thin Films," IEEE Trans. Magn. 25 (5) (1989) 3881-3883.

52. E. H. Feutrill, P.G. McCormick and R. Street, "Magnetization Behaviour in Exchange-Coupled $Sm_2Fe_{14}Ga_3C_2/\alpha$-Fe," J. Phys. D: Appl. Phys. 29 (1996) 2320-2326.

53. E. P. Wohlfarth, "Relations Between Different Modes of Acquisition of the Remanent Magnetization of Ferromagnetic Paritcles," J. Appl. Phys. 29 (1958) 595-596.

54. R. M. Bozorth, Ferromagnetism, American Telephone and Telegraph Company, 1978, reissued by IEEE Press, Piscataway, N. J. ,1993, pg. 568

55. K. D. Durst and H. Kronmüller, "Determination of Intrinsic Magnetic Material Parameters of $Nd_2Fe_{14}B$ From Magnetic Measurements of Sintered $Nd_{15}Fe_{77}B_8$ Magnets," J. Magn. Magn. Mater. 59 (1986) 86-94.

56. E. H. Feutrill, P. G. McCormick and R. Street, "Time Dependent Magnetisation in Two-Phase $Nd_2Fe_{14}B+\alpha$-Fe," Proc. of the 9th Internatinal Symposium on Magnetic Anisotropy and Coercivity in Rare-Earth Transition Metal Alloys, (São Paulo, Brazil) Sept. 5 1996, 457-463.

57. J. Wecker, K. Schnitzke, H. Cerva and W. Grogger, "Nanostructured Nd-Fe-B Magnets with Enchanced Remanence," Appl. Phys. Lett. 67 (4)(1995) 563-565.

58. M. Dahlgren, X. C. Kou, R. Grössinger, J. F. Liu, I. Ahmad, H. A. Davies and Koji Yamada, "Coercivity and Spin Reorientation Transitions in Nd-Fe-B Nanocrystalline Samples Prepared by Melt Spinning," IEEE Trans. Magn., in press.

59 M. Dahlgren, X.C. Kou, R. Grössinger and J. Wecker, "Coercivity and Magnetic Anisotropy of Nanocrystalline Nd-Fe-B Magnets Prepared by Mechanical Alloying," Proc. of the 9th Internatinal Symposium on Magnetic Anisotropy and Coercivity in Rare-Earth Transition Metal Alloys, (São Paulo, Brazil), Sept. 5 1996, 307-316.